Efficient dopants for ZrNiSn-based thermoelectric materials

1999 J. Phys.: Condens. Matter 11 1697

(http://iopscience.iop.org/0953-8984/11/7/004)

J. Phys.: Condens. Matter **11** (1999) 1697–1709. Printed in the UK PII: S0953-8984(99)99480-8

Efficient dopants for ZrNiSn-based thermoelectric materials

Heinrich Hohl†, Art P Ramirez, Claudia Goldmann†, Gabriele Ernst, Bernd Wölfing and Ernst Bucher†

Lucent Technologies, Bell Laboratories, 700 Mountain Avenue, Murray Hill, NJ 07974-0636, USA

Received 19 November 1998

Abstract. Four efficient n-type dopants have been found for ZrNiSn-based thermoelectric materials. These are Nb or Ta at the zirconium sites, and Sb or Bi at the tin sites. No suitable dopant was found for the nickel sites. In a $(Zr_{0.5}Hf_{0.5})_{0.99}Ta_{0.01}NiSn$ alloy, a power factor of $S^2\sigma = 22\ \mu W\ K^{-2}\ cm^{-1}$ and a thermal conductivity of $\kappa = 5.4 \times 10^{-2}\ W\ K^{-1}\ cm^{-1}$ were measured at 300 K, resulting in a dimensionless figure of merit $ZT = 0.12$. These values are increased to $S^2\sigma \approx 40\ \mu W\ K^{-2}\ cm^{-1}$ and $ZT \approx 0.5$ at 700 K.

1. Introduction

1.1. The thermoelectric figure of merit

In order to achieve their best performance, thermoelectric materials have to be doped. The necessity for doping becomes apparent from the expression for the thermoelectric figure of merit [1]

$$Z = \frac{S^2\sigma}{\kappa} \tag{1}$$

which is a function of the Seebeck coefficient S, the conductivity σ, and the thermal conductivity κ of a material. The numerator of this expression, $S^2\sigma$, is called the 'power factor'. Both the Seebeck coefficient and the conductivity depend strongly on the Fermi level, which in turn is a function of the carrier concentration and the temperature. An increase in the carrier concentration will generally decrease the Seebeck coefficient and increase the conductivity [2]. This means that neither insulators nor metals are good thermoelectric materials. Insulators may exhibit large Seebeck coefficients, but they lack conductivity. Metals, on the other hand, are good conductors, but their Seebeck coefficients are small. Semiconductors are located in between these two extremes, and some of them offer both a reasonably large Seebeck coefficient and a good conductivity. The result is an enhanced power factor which may be tuned to a maximum value upon doping.

The thermoelectric figure of merit of a material is also affected by its thermal conductivity. Generally, the thermal conductivity of a solid is the sum of two contributions:

$$\kappa = \kappa_L + \kappa_e. \tag{2}$$

The lattice thermal conductivity, κ_L, is caused by phonons and is a function of the temperature. The electronic thermal conductivity, κ_e, depends both on the temperature and the carrier

† Also at: Universität Konstanz, Fakultät für Physik, Fach X 910, D-78457 Konstanz, Germany.

0953-8984/99/071697+13$19.50

concentration. The latter quantity is closely related to the conductivity of the material, and in a simple model (a single band with a parabolic energy–wavenumber relation, $E \propto k^2$) this relation is described by the Wiedemann–Franz law

$$\kappa_e = L\sigma T. \tag{3}$$

The Lorentz number L depends on the Fermi level, and with increasing carrier concentration it varies between 1.11×10^{-8} V^2 K^{-2} for classical systems (intrinsic semiconductors, scattering by acoustic-mode lattice vibrations) and 2.44×10^{-8} V^2 K^{-2} for degenerate systems (heavily doped semiconductors and metals) [3].

According to the Wiedemann–Franz law, a degenerate semiconductor with a resistivity of 10^{-3} Ω cm will be accompanied by an electronic thermal conductivity of about 0.7×10^{-2} W K^{-1} cm^{-1}. The lattice thermal conductivity of most solids is much larger than this value. In these cases the electronic contribution of the thermal conductivity may be ignored, and the task of optimizing the figure of merit of a thermoelectric material upon doping is simplified to that of optimizing its power factor.

1.2. The scope of this study

This paper focuses on new thermoelectric materials which are based on ANiSn (A = Ti, Zr, Hf) compounds and their alloys. The three compounds are members of a larger family of ternary intermetallic compounds ABX, where A is a transition metal of the left-hand side of the periodic table (titanium or vanadium group elements), B is a transition metal of the right-hand side of the periodic table (iron, cobalt, or nickel group elements), and X is one of the main-group elements, Ga, Sn, or Sb. A recent compilation of all of the known ABX compounds formed by the above-mentioned elements, 54 in total, is given in reference [4].

TiNiSn, ZrNiSn, and HfNiSn crystallize in the cubic MgAgAs-type structure with lattice parameters of 5.93 Å, 6.11 Å, and 6.08 Å, respectively. This structure may be regarded as four interpenetrating fcc lattices: a lattice of A atoms and a lattice of X atoms, together forming a rock-salt structure, and a lattice of B atoms occupying the centre of every other cube. The centres of the remaining cubes are empty, thereby forming an fcc lattice of vacancies. For a graph of the unit cell and more information on compounds with the cubic MgAgAs-type structure, see reference [4].

Aliev *et al* performed resistivity measurements on ANiSn (A = Ti, Zr, Hf) and classified the compounds as narrow-band-gap semiconductors with band gaps of 0.12 eV, 0.18 eV, and 0.22 eV, respectively [5]. Shortly after, it was recognized that the compounds also exhibit large Seebeck coefficients, making them promising candidates for thermoelectric applications [6–8].

In an effort to reduce the lattice thermal conductivity of the compounds, we investigated alloys of TiNiSn, ZrNiSn, and HfNiSn [9]. It was found that $Zr_{1-x}Hf_xNiSn$ alloys form solid solutions with a reduced thermal conductivity (table 3, top section—see later). The power factors were not affected in a negative manner upon alloying.

An interesting study has been performed by Uher *et al* [10] who showed that the transport properties of the materials are rather sensitive to annealing treatments. The impact of annealing is especially conspicuous in the lattice thermal conductivity. Uher *et al* also reported Sb to be an efficient dopant for the tin sites of $Zr_{1-x}Hf_xNiSn$ alloys.

In this paper we present the results of an extended search for dopants in ZrNiSn-based thermoelectric materials. We performed our study in two steps. First, we compiled a list of potential dopants (table 1) and singled out the ones that proved efficient when introduced into ZrNiSn. In the second step, we introduced various amounts of one preferred dopant into $A_{0.5}Hf_{0.5}NiSn$ (A = Ti, Zr) alloys and determined the resulting thermoelectric figures of merit.

Table 1. Possible candidates for the doping of ANiSn (A = Ti, Zr, Hf) intermetallic compounds. Not all of the dopants have been tested. The elements Nb, Ta, Sb, and Bi are efficient n-type dopants.

Doping site	p-type	n-type
A	Sc Y La	V Nb Ta
Ni	Cr Mn Fe Co	Cu Zn
Sn	Ga In Tl	As Sb Bi

Not all of the elements listed in table 1 have been tested. In particular, arsenic and thallium seem less attractive because of their high vapour pressure and their toxicity. On the other hand, we have included some samples with a non-stoichiometric composition and performed a partial substitution for tin atoms with members of the same group, namely germanium and lead.

2. Experimental procedure

2.1. Sample preparation

The following elements formed the main constituents of our samples: titanium (Teledyne Wah Chang, 5N, crystal bar, RRR = 350), zirconium (Teledyne Wah Chang, 3N4, crystal bar, RRR = 420), hafnium (Teledyne Wah Chang, 3N4, crystal bar), nickel (MRC, grade marz, rod, RRR = 60), and tin (Cominco, 5N, pellets). The nickel and the tin pieces were etched in nitric and in hydrochloric acid, respectively, before use.

Depending on the vapour pressure of the dopants, samples were either prepared by arc melting of the elements or by a solid-state reaction in sealed quartz ampoules.

The dopants Ta, Nb, V, Y, Co, Fe, Cr, Ge, Cu, and Ga exhibit low or moderate vapour pressures. In these cases, stoichiometric mixtures of titanium, zirconium, hafnium, the dopant, and nickel were melted together in an arc furnace under a purified argon atmosphere. The congealed melt was turned over and remelted several times to ensure a homogeneous distribution of the dopant. Then a stoichiometric amount of tin was added. The reaction with tin turns the material into a semiconductor, which makes subsequent remelting more difficult because thermal strain caused by the arc tends to shatter the sample.

The buttons obtained were wrapped in tantalum foil, sealed in evacuated double-wall quartz ampoules, and annealed at either 700 °C (if the sample contained Ti)† or at 800 °C. The annealing treatment lasted between one (ANiSn compounds) and six weeks ($A_{0.5}A'_{0.5}$NiSn alloys).

The vapour pressures of In, Pb, Bi, and Sb are so high that arc melting would cause the loss of a considerable fraction of the dopant. In these cases the dopants were dissolved in tin‡. Arc-melted buttons of zirconium and nickel were crushed with a steel anvil and reacted with the doped tin solutions at 900 °C for one day. The products were powdered, pressed into pellets, and annealed at 900 °C for a week with one more intermediate grinding. The reaction and annealing steps have been performed in evacuated and sealed quartz ampoules.

Finally, both the arc-melted and the sintered samples were cut into bars with dimensions of about $1 \times 1 \times 10$ mm^3 using a diamond wheel saw.

† TiNiSn and its alloys show a weight loss if annealed above 700 °C for an extended period of time, probably caused by the loss of tin.

‡ This is except for the Bi-doped sample, which was prepared by arc melting. According to the observed weight loss, almost all of the Bi has been evaporated during the melting process.

2.2. Structural analysis

Powder diffraction patterns of the samples were recorded on a Philips PW-1710 powder diffractometer. We scanned the 2θ range of 20–100° in steps of 0.05° and at a rate of five seconds per step. Lanthanum hexaboride (JCPDS 34-427) [11] was used as a standard.

2.3. Transport measurements

Seebeck coefficients were measured with an MMR SB-100 Seebeck controller in the range 80–480 K. Linear four-probe set-ups were used for the resistivity measurements at low (4–360 K) and at elevated (290–700 K) temperatures. The resistivity measurements above room temperature were performed in an Oxysorb-purified argon atmosphere. Thermal conductivities were measured in the range 10–360 K using a steady-state method (axial heat flow apparatus). Silver epoxy was used to attach contacts to the samples in all of the transport measurements.

3. Results and discussion

3.1. Undoped and doped ANiSn ($A = Ti, Zr, Hf$)

Thermoelectric parameters of these samples at room temperature (300 K) are listed in table 2. The first section of the table shows properties of the undoped compounds; the data have been taken from an earlier study [9]. The following sections list compounds which have been doped or otherwise modified on the A site, the Ni site, and the Sn site, respectively. Resistivity curves and Seebeck coefficients of selected samples are shown in figures 1 and 2.

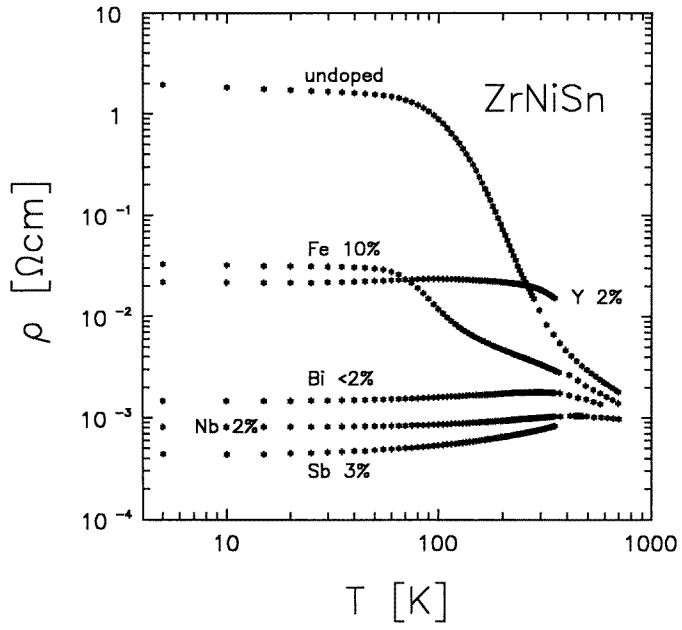

Figure 1. Resistivity curves of doped ZrNiSn compounds. The dopants and their concentrations per doping site are given.

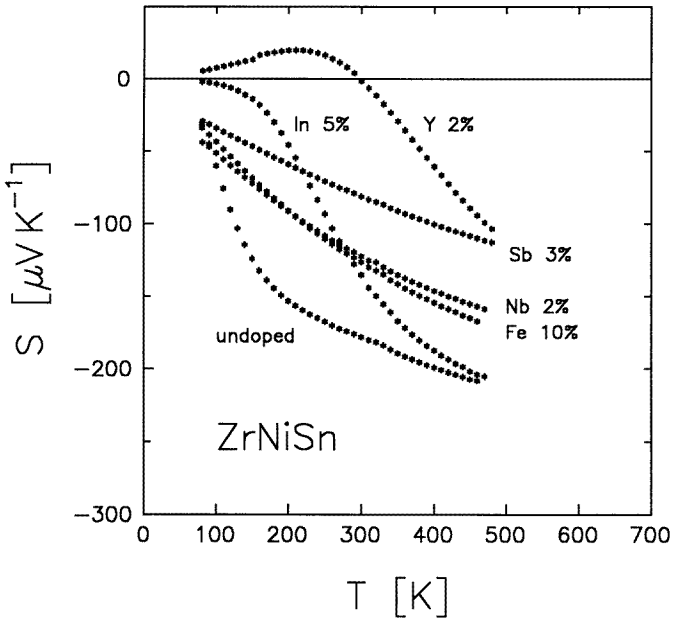

Figure 2. Seebeck coefficients of doped ZrNiSn compounds.

Table 2. Thermoelectric parameters of undoped and doped ANiSn (A = Ti, Zr, Hf) compounds at room temperature: resistivity ρ, Seebeck coefficient S, power factor $S^2\sigma$, thermal conductivity κ.

Composition	ρ (Ω cm)	S (μV K^{-1})	$S^2\sigma$ (μW K^{-2} cm^{-1})	κ (W K^{-1} cm^{-1})
TiNiSn	1.0×10^{-2}	−142	2.0	9.3×10^{-2}
ZrNiSn	1.1×10^{-2}	−176	2.8	8.8×10^{-2}
HfNiSn	1.3×10^{-2}	−124	1.2	6.7×10^{-2}
$Ti_{0.99}V_{0.01}NiSn$	2.0×10^{-3}	−164	13.2	
$Ti_{0.99}Nb_{0.01}NiSn$	1.1×10^{-3}	−126	14.4	
$Zr_{0.98}Nb_{0.02}NiSn$	1.0×10^{-3}	−121	14.5	
$Zr_{0.98}Y_{0.02}NiSn$	1.8×10^{-2}	+1	0.0	
$ZrNi_{0.98}Sn$	2.6×10^{-2}	−255	2.5	
$ZrNi_{1.02}Sn$	2.7×10^{-2}	−253	2.4	
$Zr_{1.02}Ni_{0.98}Sn$	7.4×10^{-3}	−168	3.8	
$ZrNi_{0.9}Fe_{0.1}Sn$	3.6×10^{-3}	−125	4.3	
$ZrNiSn_{0.98}$	1.4×10^{-2}	−222	3.6	
$ZrNiSn_{1.02}$	2.8×10^{-2}	−281	2.8	
$ZrNiSn_{0.9}Ge_{0.1}$	3.8×10^{-3}	−134	4.8	
$ZrNiSn_{0.9}Pb_{0.1}$	1.3×10^{-3}	−83	5.2	
$ZrNiSn_{0.97}Sb_{0.03}$	8.4×10^{-4}	−79	7.4	
$ZrNiSn_{0.98}Bi_x$	1.8×10^{-3}	−179	17.8	
$ZrNiSn_{0.98}Ga_{0.02}$	3.6×10^{-2}	−230	1.5	
$ZrNiSn_{0.95}In_{0.05}$	3.0×10^{-2}	−134	0.6	

3.1.1. Undoped compounds. In table 2 it can be seen that, in spite of their promising Seebeck coefficients, undoped ANiSn compounds are not useful for thermoelectric applications. The best commercially used thermoelectric materials combine a Seebeck coefficient of about 200 μV K^{-1}, a resistivity of about 1×10^{-3} Ω cm, and a thermal conductivity of a few 10^{-2} W K^{-1} cm^{-1} at their operating temperatures [12]. They reach or slightly exceed a dimensionless figure of merit $ZT = 1$, which is two orders of magnitude larger than the ZT-values of the undoped compounds in table 1.

3.1.2. Titanium, zirconium, or hafnium sites. Doping the titanium sites in TiNiSn with V significantly lowers the resistivity, and Nb seems to be an even more efficient dopant for this material. Niobium also works well with ZrNiSn. We have not prepared V- or Ta-doped ZrNiSn samples, but from the results listed in table 3 we may conclude that Nb may just as well be replaced by Ta, whereas V is not a good dopant when A = Zr or Hf.

The Seebeck coefficient of the Y-doped ZrNiSn shows a change in sign near room temperature. Below room temperature, the sample shows p-type behaviour, but the Seebeck coefficient is small. (It peaks at +20 μV K^{-1} near 200 K.) The resistivity of the sample shows little temperature dependence, a behaviour that is typical of a compensated semiconductor.

p-type doping of ANiSn (A = Ti, Zr, Hf) is hampered by the fact that the undoped compounds are n-type conductors with a rather high carrier concentration. At room temperature, the carrier concentration is of the order of 10^{20} cm^{-3} [10]. The addition of a p-type dopant to these materials causes the compensation of negative charge carriers. This means that positive and negative contributions to the Seebeck effect partially cancel each other.

3.1.3. Nickel site. Both a 2% deficiency and a 2% excess of nickel increase the resistivity of ZrNiSn by a factor of 2–3 over the whole temperature range. At the same time, the Seebeck coefficient is increased. The overall change in the power factor is insignificant. A sample of composition $Zr_{1.02}Ni_{0.98}Sn$ shows a slightly lower resistivity than ZrNiSn.

Four samples with nominal compositions $ZrNi_{0.9}M_{0.1}Sn$ (M = Cr, Fe, Co, Cu) have been prepared. Of these, only the Fe-doped sample shows a diffraction pattern devoid of impurity phases. In spite of the high doping level, the decrease of the resistivity is moderate in all cases.

3.1.4. Tin site. As with the nickel site, a slight non-stoichiometry in the tin site does not improve the power factor of ZrNiSn.

Substitution for tin with germanium or lead significantly lowers the resistivity of ZrNiSn. The necessary doping level, however, is rather high (10% of the tin sites), and impurity phases are visible in both diffraction patterns.

Both Sb and Bi turn out to be highly efficient n-type dopants at the tin sites. Unlike the Sb-doped sample, the Bi-doped sample has been prepared by arc melting. This (inappropriate) method vapourized most of the dopant, and the resulting composition of the sample is best described as $ZrNiSn_{0.98}Bi_x$ ($x \ll 0.02$). Nevertheless, the power factor of this sample by far exceeds that of undoped ZrNiSn.

Attempts to obtain p-type samples upon doping with Ga and In failed. With respect to the undoped compound, both the resistivity and the Seebeck coefficient of the Ga-doped sample are increased over the whole temperature range. The In-doped sample somewhat resembles the Y-doped sample described above. Its resistivity curve shows little temperature dependence, and the Seebeck coefficient appears to be shifted towards less negative values with respect to that of the undoped compound.

3.2. Undoped and doped $A_{0.5}A'_{0.5}NiSn$ (A, A′ = Ti, Zr, Hf)

A common way to reduce the lattice thermal conductivity of solids is by alloying. In solid solutions of composition $A_{0.5}A'_{0.5}NiSn$ (A, A′ = Ti, Zr, Hf), the mass disorder in the A-site lattice of the solid solutions is expected to cause additional phonon scattering, thereby reducing the lattice thermal conductivity. The strongest effect should occur near $x = 0.5$. Because Ti, Zr, and Hf are isoelectronic elements with similar electronegativities (1.3, 1.2, and 1.2, respectively), the electronic properties are not expected to change considerably because alloying does not generate a charge disorder in this lattice.

According to the results of section 3.1 there are two groups of n-type dopants for ANiSn (A = Ti, Zr, Hf) compounds. These are the group 5A elements V, Nb, and Ta, and the group 5B elements Sb and Bi. Because the group 5A elements exhibit low vapour pressures and therefore allow arc melting of the samples, we have concentrated on these dopants in the second part of our investigation. The thermoelectric parameters of undoped and doped alloys at room temperature (300 K) are listed in table 3. The first section of the table recalls the properties of undoped alloys [9]. The following sections list V-, Nb-, and Ta-doped $Zr_{0.5}Hf_{0.5}NiSn$ alloys and Nb-doped $Ti_{0.5}Hf_{0.5}NiSn$ alloys, respectively.

Table 3. Thermoelectric parameters of undoped and doped $(A_{0.5}A'_{0.5})NiSn$ (A, A′ = Ti, Zr, Hf) alloys at room temperature.

Composition	ρ (Ω cm)	S (μV K^{-1})	$S^2\sigma$ (μW K^{-2} cm^{-1})	κ (W K^{-1} cm^{-1})
$Zr_{0.5}Hf_{0.5}NiSn$	8.3×10^{-3}	−163	3.2	4.4×10^{-2}
$Ti_{0.5}Zr_{0.5}NiSn$	1.1×10^{-2}	−284	7.2	4.9×10^{-2}
$Ti_{0.5}Hf_{0.5}NiSn$	4.1×10^{-2}	−281	2.0	3.6×10^{-2}
$(Zr, Hf)_{0.990}V_{0.010}NiSn$	5.6×10^{-3}	−246	10.7	
$(Zr, Hf)_{0.999}Nb_{0.001}NiSn$	6.7×10^{-3}	−154	3.5	
$(Zr, Hf)_{0.997}Nb_{0.003}NiSn$	4.0×10^{-3}	−189	8.9	
$(Zr, Hf)_{0.990}Nb_{0.010}NiSn$	1.5×10^{-3}	−170	19.6	6.8×10^{-2}
$(Zr, Hf)_{0.990}Ta_{0.010}NiSn$	1.0×10^{-3}	−147	21.6	5.4×10^{-2}
$(Ti, Hf)_{0.999}Nb_{0.001}NiSn$	5.3×10^{-3}	−210	8.2	
$(Ti, Hf)_{0.997}Nb_{0.003}NiSn$	2.5×10^{-3}	−162	10.3	
$(Ti, Hf)_{0.990}Nb_{0.010}NiSn$	1.5×10^{-3}	−181	22.2	5.2×10^{-2}

3.2.1. Undoped alloys. The lowest thermal conductivity among those of the three alloys is found in $Ti_{0.5}Hf_{0.5}NiSn$. This result is not unexpected because of the very different atomic weights of Ti and Hf (ratio 1:3.7). The mass ratios of Zr and Hf (1:2.0) and of Ti and Zr (1:1.9) are almost the same. The fact that $Zr_{0.5}Hf_{0.5}NiSn$ shows a lower thermal conductivity than $Ti_{0.5}Zr_{0.5}NiSn$ is explained by its larger mean atomic weight. In a given class of solids, an increase in the mean atomic weight generally leads to a decrease in the lattice thermal conductivity [12]. This trend is also observed in the first section of table 2.

3.2.2. Doped $Zr_{0.5}Hf_{0.5}NiSn$. All of the alloys are single-phase materials, and their powder diffraction patterns are marked by distinct and narrow diffraction peaks (figure 3, top). Solid-solution formation in these alloys has been confirmed in an earlier study [9].

Three Nb-doped samples with doping concentrations of 0.1%, 0.3%, and 1% have been prepared. As can be seen in figure 4, an increase in the Nb content steadily lowers the resistivity.

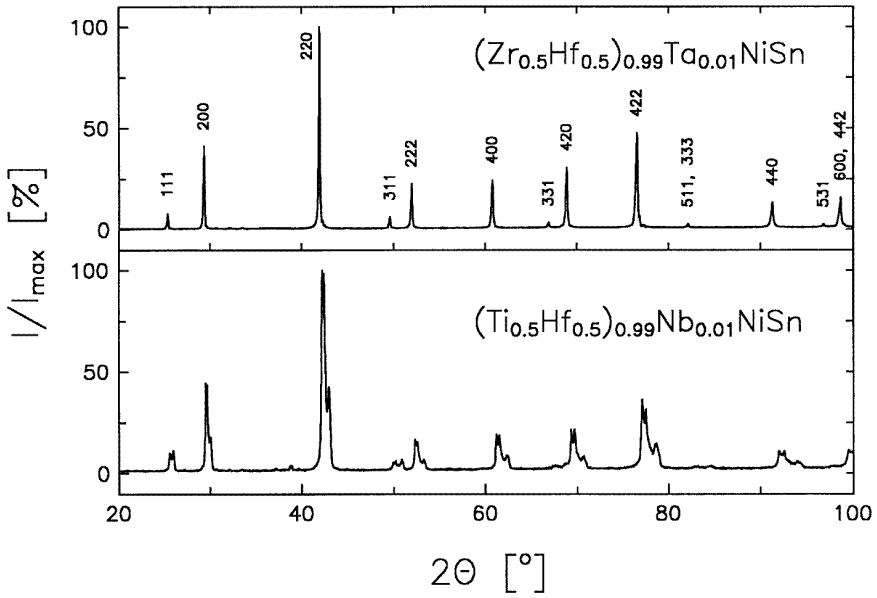

Figure 3. Powder diffraction patterns of (bottom) $(Ti_{0.5}Hf_{0.5})_{0.99}Nb_{0.01}NiSn$ and (top) $(Zr_{0.5}Hf_{0.5})_{0.99}Ta_{0.01}NiSn$, recorded with Cu K$\alpha$ radiation. The latter is a solid solution and crystallizes in the cubic MgAgAs-type structure (space group $F\bar{4}3m$, No 216) with a lattice parameter of 6.0918(2) Å.

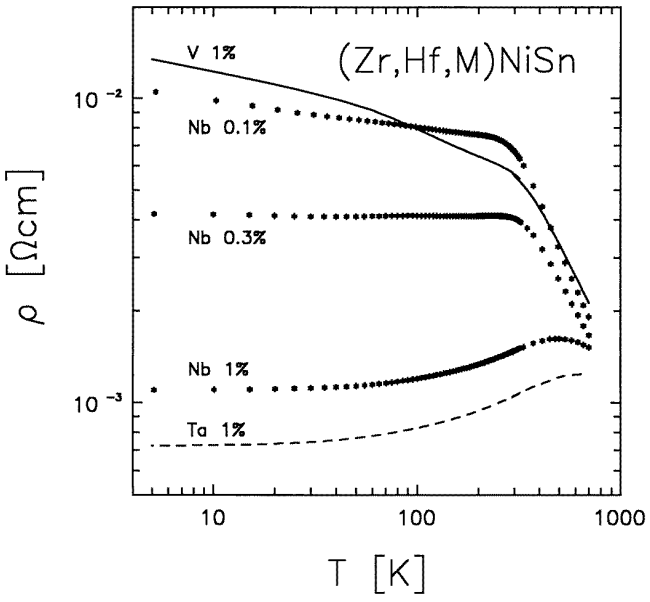

Figure 4. Resistivity curves of (Zr, Hf, M)NiSn alloys. The dopants M and their concentrations per doping site are given.

Below room temperature, the samples exhibit a semiconductor-like (0.1%), an almost constant (0.3%), and a slightly metallic (1%) temperature dependence of the resistivity. Above room

temperature, these curves slowly turn into the intrinsic semiconducting behaviour.

The resistivity curves of samples containing 1% of either V, Nb, or Ta allow one to compare the efficiency of these dopants in $Zr_{0.5}Hf_{0.5}NiSn$ alloys. It is evident that V is not a good choice in these alloys: the resistivity curve of the sample containing 1% V is close to that of the one doped with 0.1% Nb. On the other hand, the already good doping behaviour of Nb is actually surpassed by Ta.

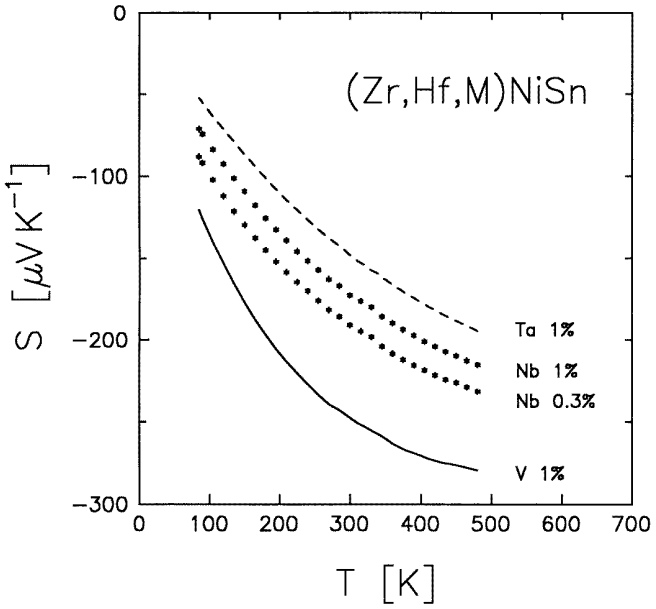

Figure 5. Seebeck coefficients of (Zr, Hf, M)NiSn alloys.

Figure 5 shows the Seebeck coefficients of the alloys. The basic rule, which states that an increase in the conductivity is accompanied by a decrease in the Seebeck coefficient, is observed in most cases. In order to calculate the power factors of the materials up to 700 K, it was necessary to extrapolate the measurements of the Seebeck coefficients. This has been done using second-degree polynomial fits to the data. The procedure of extrapolating data is not critical here because the increase in the power factors has been achieved mainly by means of an increase in the conductivities.

The calculated power factors of the alloys are shown in figure 6. The samples containing 1% Nb and 1% Ta are especially interesting. At room temperature, power factors of about 20 μW K^{-2} cm^{-1} are obtained in both cases. These values increase with temperature and reach 35 and 40 μW K^{-2} cm^{-1}, respectively, at 700 K. At this temperature, the electronic properties of the samples bear comparison with those of the best thermoelectric materials to date [12].

Below room temperature, the thermal conductivities of the samples are dominated by the lattice (figure 7). The curves peak at about 35 K. In the range 55–180 K, the temperature dependence of the curves is given by

$$\kappa \propto T^{\alpha} \tag{4}$$

with $\alpha = -0.49 \pm 0.01$ (1% Nb) and -0.51 ± 0.01 (1% Ta). Electronic contributions to the thermal conductivity emerge above 200 K and are more pronounced in the Nb-doped sample than in the Ta-doped sample.

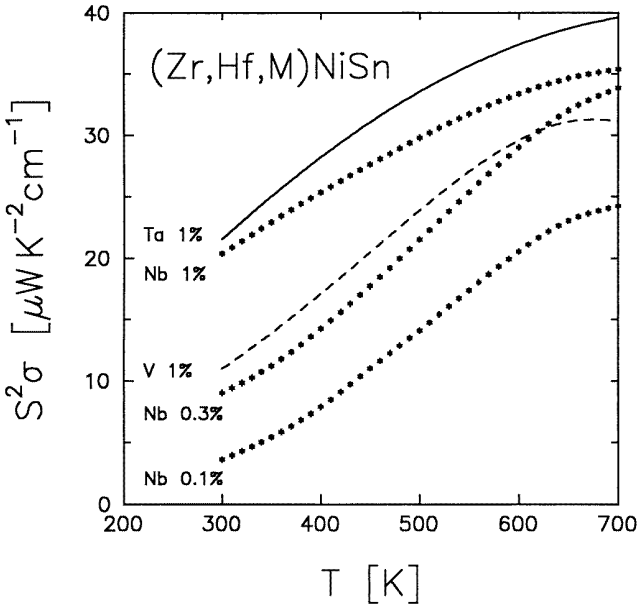

Figure 6. Power factors of (Zr, Hf, M)NiSn alloys, calculated from the data shown in figures 4 and 5.

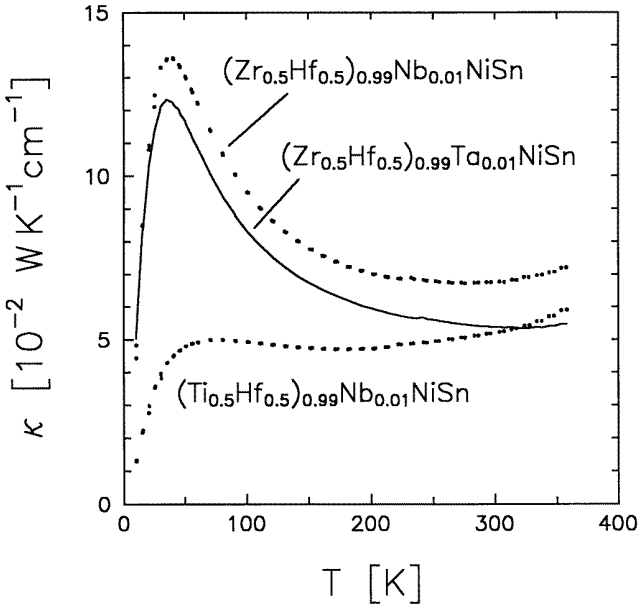

Figure 7. Thermal conductivity curves of $(A_{0.5}Hf_{0.5})_{0.99}M_{0.01}NiSn$ (A = Ti, Zr; M = Nb, Ta) alloys.

Above the Debye temperature of a solid, standard theory of the lattice thermal conductivity predicts a $\kappa_L \propto T^{-1}$ behaviour [3]. However, it has been shown by Klemens [13] that in the case of strong point defect scattering the lattice thermal conductivity varies according to

$\kappa_L \propto T^{-0.5}$. This result is based on the assumptions that the point defects scatter by virtue of their mass difference, and that the scattering of phonons by point defects exceeds the scattering by Umklapp processes.

Both conditions are obviously met by the concentrated alloys described above. A closer inspection of the ANiSn (A = Ti, Zr, Hf) compounds shows that all three of them obey equation (4) with exponents α of about -0.7. This leads to the conclusion that point defect scattering is also present in these compounds, probably caused by a partial mutual substitution of A and Sn atoms.

Combining the room temperature data of table 3, dimensionless figures of merit $ZT = 0.08$ and 0.12 are obtained for $(Zr_{0.5}Hf_{0.5})_{0.99}Nb_{0.01}NiSn$ and $(Zr_{0.5}Hf_{0.5})_{0.99}Ta_{0.01}NiSn$, respectively. These values exceed those for the undoped ANiSn (A = Ti, Zr, Hf) compounds by one order of magnitude, but they are still an order of magnitude too small for applications.

A better performance is found above room temperature. Assuming that the thermal conductivity of the Ta-doped sample does not increase much above room temperature, $ZT \approx 0.5$ is achieved at 700 K. This differs from the value for the best materials only by a factor of two and gives hope for further improvement.

3.2.3. Doped $Ti_{0.5}Hf_{0.5}NiSn$. The powder diffraction patterns of these alloys are marked by broad diffraction peaks, some of them split up into doublets or triplets (figure 3, bottom). Similar patterns are obtained for alloys of TiNiSn and ZrNiSn. The quality of the diffraction patterns is not sufficiently good to allow a refinement of the lattice parameters. It is not clear whether these patterns are caused by a structural distortion or whether the alloys are two-phase mixtures of titanium-rich and titanium-poor solid solutions. Changes in the annealing treatment do not improve the quality of the patterns.

The electronic properties of the Nb-doped $Ti_{0.5}Hf_{0.5}NiSn$ alloys are very similar to those of the corresponding $Zr_{0.5}Hf_{0.5}NiSn$ solid-solution series. With increasing Nb content, the resistivity of the alloys is lowered and the power factor increased. The sample containing 1% Nb shows power factors of 22 μW K^{-2} cm^{-1} (300 K) and about 32 μW K^{-2} cm^{-1} (700 K). The temperature dependence of the thermal conductivity is shown in figure 7. The almost total suppression of the low-temperature peak in the lattice thermal conductivity is remarkable. It is also notable that electronic contributions to the thermal conductivity become rather prominent above room temperature.

4. Conclusions

Niobium, tantalum, antimony, and bismuth are efficient n-type dopants for ZrNiSn-based thermoelectric materials. The first two dopants have the benefit of a very low vapour pressure and allow the preparation of samples via arc melting. A solid-state reaction of powdered materials in sealed quartz ampoules is necessary when doping with Sb or Bi. p-type doping of the materials is hampered by the high electron concentration present in the undoped compounds. No suitable dopants have been found for the nickel sites, nor did slight deviations from the ideal stoichiometry increase the power factor.

When about 1% of an n-type dopant is added to the materials, the temperature dependence of the resistivity changes from showing a semiconductor-like behaviour to showing a metallic one. Although the resistivity is lowered considerably, the reduction in the Seebeck coefficient is still tolerable because the power factor $S^2\sigma$ is improved by about one order of magnitude. At room temperature, power factors of about 20 μW K^{-2} cm^{-1} are reached, and a maximum value of 40 μW K^{-2} cm^{-1} has been achieved at 700 K.

The promising electronic properties of ZrNiSn-based thermoelectric materials are complemented by the ease of sample preparation and processing. Samples may be prepared from the elements by arc melting, and the resulting buttons are mechanically sturdy. They may be cut with a diamond blade saw in water and are easily polished with sandpaper. Reliable contacts to the samples are obtained with silver epoxy or by soldering with tin.

For comparison, both Bi_2Te_3 and PbTe are rather soft and they are easily deformed mechanically. Silver epoxy contacts to these materials are not always reliable. Bi_2Te_3 also tends to cleave because of its layered structure. Both materials are therefore only being used in sintered form.

The main drawback of the ZrNiSn-based thermoelectric materials is their high lattice thermal conductivity. Although alloying of ZrNiSn with HfNiSn causes a reduction in the lattice thermal conductivity, the impact is not sufficient to obtain the figure of merit $ZT \approx 1$ which is necessary for applications.

In fact, it appears that the most impressive feature of currently used thermoelectric materials is their low lattice thermal conductivity. With room temperature lattice thermal conductivities of (1–1.6) $\times 10^{-2}$ W K^{-1} cm^{-1} (Bi_2Te_3-based alloys), 2×10^{-2} W K^{-1} cm^{-1} (PbTe-based alloys), and 3.3×10^{-2} W K^{-1} cm^{-1} (Ge–Si alloys) [12], these materials are very poor conductors of heat. For comparison, the thermal conductivities of stainless steel type 304 and of Pyrex-type glasses are 15×10^{-2} W K^{-1} cm^{-1} and 1.1×10^{-2} W K^{-1} cm^{-1}, respectively [14].

Some new concepts as regards reducing the lattice thermal conductivities of solids have been proposed by Slack [15,16]. The most intriguing idea is based on atoms that are 'rattling' in oversized voids of a crystal structure, or on weakly bound atoms that are 'wobbling' back and forth between two positions. The efficiency of the first-mentioned approach has been demonstrated for filled skutterudites, a new class of thermoelectric material based on compounds such as $CoSb_3$ [17]. The cubic MgAgAs-type structure of ZrNiSn offers a sublattice of voids. These voids are, however, much smaller than the ones in $CoSb_3$. If it were to be possible to reduce the lattice thermal conductivity of doped ANiSn (A = Ti, Zr, Hf) by a method similar to that used in the case of the filled skutterudites, an outstanding thermoelectric material would be obtained. There is a demand for a high-performance n-type thermoelectric material with an operating temperature around 700 K, because the best thermoelectric materials to date, TAGS-80 and TAGS-85, are both p-type without equivalent counterparts. (TAGS is an acronym for tellurium, antimony, germanium, and silver.) The materials are two-phase alloys of $AgSbTe_2$ and GeTe (80–85%) and reach ZT-values of 1.6 and 1.4, respectively, at 700 K [18].

Acknowledgments

We would like to thank the Teledyne Wah Chang company in Albany, OR, for generous support in providing high-purity titanium, zirconium, and hafnium crystal bars. The authors are also grateful to Dr B Batlogg for helpful discussions.

References

[1] Goldsmid H J 1995 Conversion efficiency and figure-of-merit *CRC Handbook of Thermoelectrics* ed D M Rowe (Boca Raton, FL: Chemical Rubber Company Press) pp 19–25

[2] Bhandari C M and Rowe D M 1995 Optimization of carrier concentration *CRC Handbook of Thermoelectrics* ed D M Rowe (Boca Raton, FL: Chemical Rubber Company Press) pp 43–53

[3] Goldsmid H J 1965 *The Thermal Properties of Solids* (New York: Dover)

[4] Hohl H, Ramirez A P, Goldmann C, Ernst G, Wölfing B and Bucher E 1998 New compounds with MgAgAs-type structure: NbIrSn and NbIrSb *J. Phys.: Condens. Matter* **10** 7843–50

[5] Aliev F G, Brandt N B, Moshchalkov V V, Kozyrkov V V, Scolozdra R V and Belogorokhov A I 1989 Gap at the Fermi level in the intermetallic vacancy system RNiSn (R = Ti, Zr, Hf) *Z. Phys.* B **75** 167–71

[6] Aliev F G, Kozyrkov V V, Moshchalkov V V, Scolozdra R V and Durczewski K 1990 Narrow band in the intermetallic compounds MNiSn (M = Ti, Zr, Hf) *Z. Phys.* B **80** 353–7

[7] Cook B A, Harringa J L, Tan Z S and Jesser W A 1996 TiNiSn: a gateway to the (1, 1, 1) intermetallic compounds *Proc. ICT96: 15th Int. Conf. on Thermoelectrics* (Piscataway, NJ: IEEE) pp 122–7

[8] Kloc Ch, Fess K, Käfer W, Friemelt K, Riazi-Nejad H and Bucher E 1996 Crystal growth of narrow gap semiconductors for thermoelectric applications *Proc. ICT96: 15th Int. Conf. on Thermoelectrics* (Piscataway, NJ: IEEE) pp 155–8

[9] Hohl H, Ramirez A P, Kaefer W, Fess K, Thurner Ch, Kloc Ch and Bucher E 1997 A new class of materials with promising thermoelectric properties: MNiSn (M = Ti, Zr, Hf) *Materials Research Society Symp. Proc.* vol 478, ed T Tritt *et al* (Pittsburgh, PA: Materials Research Society) pp 109–14

[10] Uher C, Hu S, Yang J, Meisner G P and Morelli D T 1997 Transport properties of ZrNiSn-based intermetallics *Proc. ICT97: 15th Int. Conf. on Thermoelectrics* (Piscataway, NJ: IEEE) pp 485–8

[11] *JCPDS—International Centre for Diffraction Data* 1995 PC-PDF Card Retrieval/Display System, version 2.16 (Newtown Square, PA: International Centre for Diffraction Data)

[12] Wright D A 1970 Materials for direct-conversion thermoelectric generators *Metall. Rev.* **15** 147–60

[13] Klemens P G 1960 Thermal resistance due to point defects at high temperatures *Phys. Rev.* **119** 507–9

[14] Lide D R 1995 Thermal conductivity of glasses *CRC Handbook of Physics and Chemistry* 76th edn, ed D R Lide *et al* (Boca Raton, FL: Chemical Rubber Company Press) section 12, pp 12–181

Lide D R 1995 Commercial metals and alloys *CRC Handbook of Physics and Chemistry* 76th edn, ed D R Lide *et al* (Boca Raton, FL: Chemical Rubber Company Press) section 12, pp 12–190

[15] Slack G A 1995 New materials and performance limits for thermoelectric cooling *CRC Handbook of Thermoelectrics* ed D M Rowe (Boca Raton, FL: Chemical Rubber Company Press) pp 407–40

[16] Slack G A 1997 Design concepts for improved thermoelectric materials *Materials Research Society Symp. Proc.* vol 478, ed T Tritt *et al* (Pittsburgh, PA: Materials Research Society) pp 47–54

[17] Sales B C, Mandrus D and Williams R K 1996 Filled skutterudite antimonides: a new class of thermoelectric materials *Science* **272** 1325–8

[18] Skrabek E A and Trimmer D S 1997 Properties of the general TAGS system *CRC Handbook of Thermoelectrics* ed D M Rowe (Boca Raton, FL: Chemical Rubber Company Press) pp 267–75